

EFFECT OF NON-RECTANGULAR BLADE TIPS ON BVI NOISE

FOR A TWO-BLADED ROTOR

M. SCHAFFAR, J. HAERTIG, P. GNEMMI

Institut Franco-Allemand de Recherches de Saint-Louis

12 rue de l'industrie

68301 SAINT-LOUIS (France)

Abstract

The vortex lattice method jointly used with a local conformal mapping (to transform the thin blade into a thick one) is briefly described. This method is now applied to a two-bladed rotor with several blade tips (rectangular, forward or backward swept, anhedral, progressive swept, progressive swept and anhedral). The effect of these blade tips on the emitted noise is calculated with an acoustic code which is based on the Ffowcs-Williams-Hawkings (FW-H) equation .

Two flight conditions are explored. The aerodynamic results (thrust curve, wake evolution, vortex shedding) are analysed. The noise directivities and the individual pressure signatures show that the PF1 blade tip is interesting for one flight case while the PF2 seems to be interesting for the second flight case. Nevertheless, for these two blade tips a decrease (1 to 2 dB) in noise in the rotor plane is obtained (that means especially a reduction of the thickness noise) and a short reduction (1 dB) is also obtained below the rotor plane for the BVI noise in the forward direction.

Notation

a_0	sound speed
C_p	pressure coefficient
C_T	thrust coefficient
(i,j)	index, chordwise and spanwise
l_r	component of the loading vector in the observer direction
M_r	Mach number in the observer direction
N, N_x, N_y	panel number (total, chordwise, spanwise)
$p(x,t)$	acoustic pressure
R	rotor radius
r	distance between the blade element and the observer

$\vec{r}_{i,j}$	distance between the panel i and the panel j
$S_{i,j}$	surface of the panel (i,j)
t	observer time
U_∞, U_x	velocity of the ambient air
V_n	normal velocity component
$\vec{V}_{i,j}$	velocity vector for the control point of the panel (i,j)
x	observer position
β_j^k	circulation shedded in the wake
$\Gamma, \Gamma_{i,j}^n, \gamma_{i,j}^n$	panel bounded circulation
μ	advancing coefficient
ϕ	potential
Φ	angle below the rotor plane
Ψ	azimuth angle in the rotor plane
ρ	air density
τ	source time ($=t-r/a_0$)
θ	pitch angle
θ_c, θ_s	cyclic pitch
Θ	angle in an horizontal plane for the noise directivity
Ω	angular rotational velocity

1. Introduction

Rotor blade-vortex interaction (BVI) noise is one between several noise sources for helicopters in flight ; it is caused by unsteady airloads induced on the blades by the vortical wake of previous blades.

Many theoretical and experimental studies have been achieved in the last ten years. Now, it is known that the BVI noise has a strong forward directivity and that it depends very closely on the flight parameters. One way to reduce the rotor noise is to build blades with non-rectangular tips and especially blades with anhedral tips or with winglets. Some experiments with this type of

blades have been already achieved ([1,3]). For example, the fixation of a winglet at the blade tip produces a spreading of the tip vortex and a decrease of its position with respect to the blade during the BVI in comparison with a rectangular blade tip; in this case one can expect a decrease in the BVI Noise ([1]). A decrease of 1 dB of the rotor noise was measured in the rotor plane for blades named PF1([2,3], ONERA).

In this paper we present an application of our method (based on the Vortex Lattice Method and on the Ffowcs-Williams-Hawkings equation, [4]) in the case of the rotor noise in the rotor plane and below for several blade tips like those used at the ONERA (for high-speed rotors). In the following sections, we will describe briefly the Vortex Lattice Method (VLM) and the acoustic code. Finally we present the results obtained for a two-bladed rotor in two advancing flight cases for 6 blade tips: rectangular, forward swept(30°), backward swept(30°), anhedral (-10°), progressive swept (PF2), progressive swept and anhedral (PF1).

2. Description of the computational method

Description of the VLM

The VLM is an extension to the 3D case of 2D methods based on potential flow with point vortices and the same basic assumptions are made: incompressible and inviscid flow. Each of the two blades is divided into $N = N_x \cdot N_y$ rectangular or quadrilateral panels ($N_x = 12$ chordwise, $N_y = 14$ spanwise). On this panel system, we put a bound vortex lattice with vortex lines in span direction of the strength $\Gamma_{i,j}^n$ (figure 1) and vortex lines in chord direction of the strength $\gamma_{i,j}^n$, defined by:

$$\gamma_{i,j}^n = \sum_{k=1}^i (\Gamma_{k,j-1}^n - \Gamma_{k,j}^n) \quad (1)$$

where n indicates the time step.

With the no-penetration condition applied in the moving frame, the following system is obtained in the fixed frame for the time step n:

$$[\vec{V}_{i,j}(\Gamma_{i,j}^n, \gamma_{i,j}^n) + \vec{V}_{i,j}(\text{wake}) + \vec{\Omega} \wedge \vec{r}_{i,j} + \vec{U}_\infty] \cdot \vec{n}_{i,j} = 0 \quad (2)$$

$$\forall_{i,j} \quad \begin{matrix} i = 1, N_x \\ j = 1, N_y \end{matrix}$$

The two first terms in (2) are the velocities induced by the blade-bounded vortices ($\Gamma_{i,j}^n$ and $\gamma_{i,j}^n$) and by the free vortices (wake); $\vec{\Omega} \wedge \vec{r}_{i,j}$ is the rotation velocity at the control point of the panel (i,j). At each time step the conservation of the circulation is warranted by the shedding of an unsteady vortex line β^n .

The wake lattice is built stepwise with the vortices β_j^k and γ_j^k (previously shedded) whose circulation remains constant.

The system of N linear equations is built by writing the induced velocities at each control point (which follows the rule of Pistoiesi, 1/4, 3/4, see figure 2). The Biot-Savart law gives the induced velocity for a line vortex (figure 3):

$$\vec{v}_{\text{ind}} = \frac{\Gamma}{4\pi} \frac{(\cos \alpha + \cos \beta)}{r} \frac{\vec{AB} \wedge \vec{AM}}{|\vec{AB} \wedge \vec{AM}|} \quad (3)$$

In the equation (3) we have a source of numerical problems if the distance r is too small. The regularization method used here neglects the segment for a distance r smaller than a given threshold (cut-off length) which needs to be chosen carefully; in the following computations, the cut-off length is 0.5 chord.

The pressure jump across the blades $\Delta p_{i,j} = -(p_\ell - p_u)_{i,j}$ is obtained with the Bernoulli equation written for the upper (u) and the lower (ℓ) side of the wing:

$$-\left(\frac{p_\ell - p_u}{\rho}\right)_{i,j} = \left[-\frac{\partial(\varphi_u - \varphi_\ell)}{\partial t} + \frac{U_\ell^2 - U_u^2}{2} \right]_{i,j} \quad (4)$$

With the definition of the potential φ and the relation $\vec{u} = \text{grad}(\varphi)$ we determine the expressions above by using the singularities $\Gamma_{i,j}$ and $\gamma_{i,j}$.

At the end of the time step n , the normalized rotor thrust coefficient C_T is computed (we take $\rho = 1$) with:

$$C_T(t) = \left(\sum_{i,j} \Delta p_{i,j} S_{i,j} \right) / (\pi R^2 (\Omega R)^2) \quad (5)$$

Description of the method used to thicken the blade

The acoustic prediction of the loading noise based on FW-H equation needs the local loads (strength and direction) acting upon a thick blade.

At each time step the following assumption is made: for each position in span a conformal mapping can be used to extrapolate the results to a thick blade assuming that the potential φ re-

mains the same. We use for example a Joukowski transformation (thickness ε , chord 1). The potential φ is obtained by integrating the velocity along a line coming from infinity, 10 spans in z -direction to the inner LE (leading edge) and by adding (upper side) or by subtracting (lower side) half of the encountered singularity $\Gamma_{k,j}^n$ from one control point to the next.

The pressure coefficient $(C_p)_{u,e}$ is then calculated for the upper and the lower side of the "thick" blade.

BVI noise prediction

Starting from the well-known Ffowcs-Williams-Hawkings equation and following the integration of Lawson, the fluctuation of the acoustic pressure for the loading noise can be expressed with the following equation:

$$4\pi p(\vec{x}, t) = + \int_S \left[\frac{1}{a_0 r (1 - M_r)^2} \left\{ \frac{\partial \ell_r}{\partial \tau} + \ell_r \frac{\partial M_r}{\partial \tau (1 - M_r)} \right\} \right]_+ dS \quad (6)$$

In the same way, the acoustic pressure for the thickness noise is expressed by:

$$4\pi p(\vec{x}, t) = + \int_S \left[\frac{1}{(1 - M_r)} \frac{\partial}{\partial \tau} \rho_0 \frac{V_n}{r(1 - M_r)} \right]_+ dS \quad (7)$$

where M_r is the Mach number of the element dS relating to the observer, r is the distance between dS and the observer, ℓ_r is the component of the loading vector $\vec{\ell}$ in the observer direction (which represents the load acting from the blade on the ambient fluid), τ is the emission time ($= t - r/a_0$) at which the terms in $[]_+$ have to be evaluated, a_0 is the sound speed, V_n is the scalar product between the velocity on the blade and the interior normal vector for the surface element dS .

The noise is computed in the time domain (this is more faster than a computation in the frequency domain) with a code similar to that used by Farrasat [5] which is based on the MIT code for subsonic tip speed propellers. The noise is computed with the far field formulation and then

adjusted for the real distance r . For the aerodynamic calculation, the time step is 5° whereas it is 2° for the acoustic calculation, the pressure coefficients being interpolated in the acoustic code.

2. Application to a two-bladed advancing rotor

The rotor used here is the two-bladed AH1-OLS model rotor [6]. The dimensionless characteristics are the following: chord 1., rotor radius $R = 9.22$, root distance 1.678, linear twist 10° , collective pitch 4.73° , coning angle 0° , advancing coefficient $\mu = 0.164$, rotational angular velocity $\Omega = (0., 0., 0.6632)$, tip path plane angle 2° ,

free stream velocity equal to 1., thickness coefficient 9.7%.

The results presented in reference [6] are in-flight tests and wind-tunnel tests but we take into only account the wind-tunnel tests ($\mu = 0.164$, $C_T = 0.0054$). For the cyclic pitch, we have chosen the following 2 cases: 1) $\theta_c = 1^\circ 97$, $\theta_s = 1^\circ$, 2) (the experimental) $\theta_c = 1^\circ$, $\theta_s = 1^\circ 97$. The wind-tunnel velocity is 36.9 m/s and the real chord is 0.104 m in both cases.

The tested blade tips are the following (figure 4): 1) rectangular tip (Rect), 2) 30° backward swept tip (Bws), 3) 30° forward swept tip (Fws), 4) an anhedral (-10°) tip (Anh), 5) progressive swept tip (PF2), 6) progressive swept and anhedral (PF1). These blade tips are especially designed for high speed rotors but we thought it being interesting to check the effect of these tips on the rotor noise emission (in-plane noise and BVI noise).

2.1 Test case 1 : Aerodynamic results

Figure 5 shows the evolution of the thrust curve for the Rect, Anh and PF2 tips. The mean value of the thrust coefficient seems not to be a function of the blade tip. The values are the following: 0.005313 (Rect), 0.005276 (Bws), 0.005345 (Fws), 0.005234 (Anh), 0.005275 (PF2), 0.005158 (PF1); some differences are found only when the blades are interacting with the wakes.

The variation of the tip vortex is shown in figure 6 for the Rect and the Anh tips (the results for the tips Rect, Bws, Fws, PF2 are similar). The biggest differences are found for the Anh tip (and obviously for the PF2 tip too): when the blade is parallel to the free stream velocity the circulation is lower on the retreating side (RS) and stronger on the advancing side (AS) in comparison with the Rect tip. This singular behaviour is an effect of the anhedral shape: on the AS the spanwise component of the normal velocity is added to the free stream velocity and this produces a stronger singularity (and a stronger tip vortex) while on the RS this same component is subtracted from the free stream velocity (so it gives a lower singularity and a lower tip vortex).

Further the analysis of the vortex curve, in relation to the blade vortex interaction gives, the following result: the vortex line shedded for the azimuth an-

gles from 465° to 535° (with the strongest circulation) corresponds to the advancing side interaction for the azimuth angle 775°. In this case, it is clear that a reduction of this vortex shedding ($\Psi = 465^\circ$ to 535°) can produce a reduction of the BVI noise.

We have also analysed the position of the wake vortex lines (figure 7) during the BVI for $\Psi = 775^\circ$ at 0.84R, the mean distance in front of the blade is 2.1 chord and the mean height is -0.5 chord for all blade tips; at 0.96R, the mean distance ahead the blade is 1.4 chord and the height is -0.6 chord. Consequently, we have not found any significant deviations between the blade tips as regards the wake position during BVI.

Figure 8 shows the distribution of the circulation times $100./(\Omega R^2)$ over the rotor disk during one revolution for the Rect blade tip: this figure is obtained by summing up the singularities in the chordwise direction for each position in span and for each azimuth angle with a step of 5°. An UNIRAS plot routine is then used to obtain the iso-circulation lines shown in figure 8. One can see two "mountains" on the advancing side: one near $\Psi = 0^\circ$ and $r/R = 0.5$, the second for $\Psi = 100^\circ$ to 160° and $r/R = 0.5$ to 0.9. Only the last mountain of circulation is to be considered, because the shedded circulation which will produce the BVI depends on it! It is also clear that the circulation is low on the retreating side.

This type of figure has been drawn for all blade tips. All figures are practically similar except those obtained for the anhedral blade tips (tip 4 and 6). To enhance the differences, figure 9 shows the subtraction (Anh-Rect): it is quite clear that the anhedral shape produces a serious decrease of the circulation on the rotor disk for $\Psi = 90^\circ$ to 270° in the vicinity of the blade tip ($0.8 < r/R < 1.$).

Figures 10 and 11 show the circulation shedded in the wake (along the emission line) for each azimuth angle during one rotor revolution and for the Rect and PF1 tips. We see the same two regions (as before) with a strong circulation but the second region is more extended. The fact noticed before (see figure 6) that the shedded circulation of the anhedral blade tip is stronger on the AS and weaker on the RS appears only clearly for $\Psi = 120^\circ$ to 270° on the AS! Another fact to be noticed is a strong negative circulation near the

root of the blade: this circulation may be unrealistic and destroyed by the rotor hub, but it is up to now given by the solution of the system of equations.

In figure 12 it is shown the gradient of the circulation shedded in the wake for the Rect tip. As expected, the maximum of the gradient is obtained at the end of the blade, otherwise the gradient is low and negative (near the root). In this case all blade tips give the same picture.

2.2 Test case 1 : Acoustics results

First we have calculated the horizontal directivities in the rotor plane and below for all blade tips. Figures 13 to 17 show the curves. The following angles are used: $\Theta (>0 \text{ C-CW})$ is the angle in the horizontal plane with its origin in the forward direction, Φ is the angle below the rotor plane (<0 downwards) with its origin in the horizontal plane.

In the rotor plane, the thickness noise has its maximum in the forward direction (Θ near 0°); four blade tips (Rect, Bws, Fws, Anh) give nearly the same result except the PF1 and PF2 tips, where a significant noise reduction (-2 dB) is obtained. This reduction is much more due to the blade surface reduction than to the particular form.

The loading noise seems to have its maximum in two directions: in the the forward direction ($\Theta = 0^\circ$ to 30°) and for Θ near 290° . The curves show a very irregular shape, and the best noise reduction in the forward direction is always obtained for the PF1 and PF2 tips. The other blade tips (Bws, Fws, Anh) do not seem to be very efficient in the loading noise reduction, because in some azimuth angles the noise is stronger than for the rectangular blade.

Figure 15 shows the directivities obtained for the total noise. In this case also a strong forward maximum is found; a noise reduction is obtained for the two blade tips PF1 and PF2 but the best blade tip is the PF1 for $\Theta = 30$ to -30° and the PF2 one for $\Theta = -30$ to -75° with a reduction of nearly 2 dB in comparison with the rectangular blade.

For 30° below the rotor plane, we only consider the total noise because the thickness noise is near to

zero. Figure 16 shows the curves calculated for this case: the general shape of the directivity looks like a bean which has two directions for the maximum noise emission, Θ near 20° and Θ near 300° , both in forward direction. A direction with minimum noise emission is found for $\Theta = 330^\circ$. For the blade tips the results are the following: in comparison with the Rect tip, the tips Bws, Fws, Anh, PF1 give an increase of the noise emission while the PF2 tip gives a little reduction.

For the other angles below the rotor plane (see figure 17 for -45°), all blade tips give practically the same result with a short advantage for the PF2 tip.

Some pressure signatures are presented in the figures 18 to 20 for the loading noise, the thickness noise and the total noise in the forward direction for $\Phi = 0^\circ, -30^\circ$ and -45° . In this case one can see some differencies between the blade tips: the number of the peaks and their amplitude are variable. For the thickness noise which looks like a negative peak, the noise reduction noticed before for the PF2 tip is obvious.

3.2 Test case 2 : Aerodynamic results

As shown before, for the second test case the cyclic pitch is the following: $\theta_c = 1^\circ, \theta_s = 1^\circ 97$. For this test we have only used the Rect, PF2 and PF1 blade tips, which have been the most efficient in the first study.

The thrust coefficient shown in the figure 21 has a shape similar to that obtained in the first case, but the oscillations are stronger. Nevertheless, the mean values are practically the same as before : 0.005345 (Rect), 0.005400 (PF2), 0.005256 (PF1). The tip vortex given in the figure 22 shows that the peak value is stronger than before and that the PF1 tip gives always a smaller circulation (the anhedral effect).

For the distribution of the normalized circulation on the rotor disk (shown in figure 23 for the rectangular tip), the pictures are similar for the three blade tips: with respect to the first test case, the circulation is stronger and the two "mountains" are more extended. The circulation shedded in the wake (see figure 24) for the rectangular tip looks like that obtained for the first test case.

3.3 Test case 2 : Acoustic results

The horizontal directivities in the rotor plane and below are shown in figures 26 to 29.

On an average we see that the second flight test gives less noise than the first:

- in the rotor plane: -2 dB for the maximum of the thickness noise and of the loading noise, -1.5 dB for the total noise except for the PF2 tip.
- below the rotor plane, -1 dB for $\Phi = -30^\circ$.

The comparison of the three blade tips gives the following results:

- the maximum of the noise emission is always obtained in the forward direction;
- in the rotor plane, the PF1 and PF2 tips give a thickness noise lower (-2 dB) than the Rect tip; for the loading noise, the greatest reduction (with -3 to -5 dB) is obtained for the PF1 tip; finally, for the total noise, the PF2 tip gives a noise increase (+2 dB) in the forward direction and the PF1 tip gives a noise reduction of 1.5 dB with respect to the Rect tip;
- below the rotor plane, the PF1 tip gives always a reduction of 1 dB while the PF2 tip is comparable to the Rect tip.

Some noise signatures presented in figures 30 to 32 show the same results as given before. They confirm the efficiency of the PF1 blade tip for the noise reduction in the rotor plane end below.

4. Concluding remarks

The vortex lattice method explained in this paper seems to be a good method for the aerodynamic calculation of the rotor loads which serve as an

input for an acoustic code used for the noise prediction.

This method was applied for the noise prediction (in- plane noise and BVI noise) for several "advanced" blade tips like those used for high speed rotors.

For the AH1-OLS model rotor used here for the two test cases (advancing flight ($\mu = 0.164$) and two cyclic pitches ($1 = > \theta_c = 1^\circ 97, \theta_s = 1^\circ, 2 = > \theta_c = 1^\circ, \theta_s = 1^\circ 97$), the results are the following:

- the thrust coefficient shows only small deviations (1 to 3%) with respect to the blade tip;
- the aerodynamic results look the same for all blade tips except for the anhedral and PF1 tips where the tip vortex is lower on the retreating side and stronger on the advancing side;
- all noise directivities in the rotor plane and below give a maximum of the noise emission in the forward direction;
- in comparison with the rectangular blade tip, the thickness noise can be reduced (-2 dB) with the PF2 blade tip for one test case and with the PF1 blade tip for the second test case; in the same way the loading noise is reduced (-1 dB) for the two blade tips; the total noise is also reduced (-2 dB) for some azimuth angles in the forward direction;
- below the rotor plane, the noise reduction is a little weaker, -1 dB for the PF1 and PF2 blade tips;
- for the following blade tips (backward swept, forward swept, anhedral) the results do not give any noise reduction, sometimes however a noise increase is obtained.

In the future this method (VLM with local conformal mapping) can be applied to a three- or four-bladed rotor and the high harmonic control can also be studied with the VLM.

BIBLIOGRAPHY

- [1] R.H.G. MULLER
Winglets on rotorblades in forward flight.
A theoretical and experimental investigation
Fourteenth European Rotorcraft Forum, Paper 10, Milano, 20-23 Sept 1988
- [2] M. COSTES, A. DESOPPER., P. CERONI and P. LAFON
Flow field prediction for helicopter rotor with advanced blade tip shapes using CFD techniques
2nd Int.Conf. on Basic Rotorcraft Research
College Park, Univ.of Maryland, 16-18 feb.1988
- [3] A. DESOPPER., P. LAFON, JJ PHILIPPE and J. PRIEUR
Effect of an anhedral sweptback tip on the performance of a helicopter rotor
44th Annual Forum and Technology Display, AHS, Washington , 16-18 june 1988
- [4] M. SCHAFFAR, J. HAERTIG and P. GNEMMI
Aerodynamic loads and blade vortex interaction noise prediction
Fifteenth European Rotorcraft Forum, Paper 3, Amsterdam, 12-15 sept 1989
- [5] F. FARASSAT and G.P. SUCCI
A review of propeller discrete frequency noise. Prediction technology with emphasis on two current methods for time domain calculations
Journal of Sound and Vibration, 1980, 71, 3, pp.399-419
- [6] W.R. SPLETTSTOESSER, K.J. SCHULTZ, D.A. BOXWELL, F.H. SCHMITZ
Helicopter model rotor blade vortex interaction impulsive noise: scalability and parametric variation
NASA TM 86007 Dec.1984

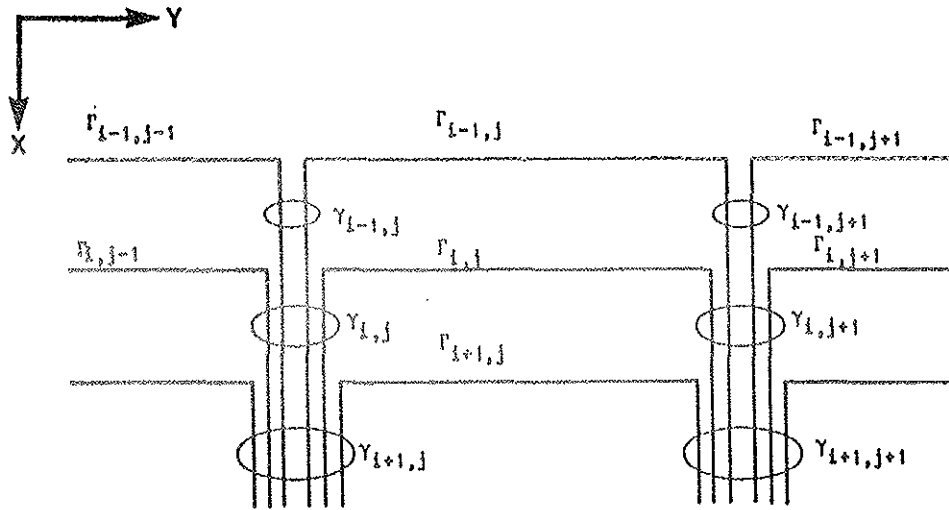


FIG.1 : Sketch for the Vortex Lattice on the blade

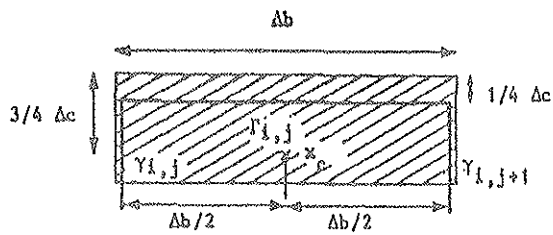


FIG.2 : Position of the vortex line and the control point

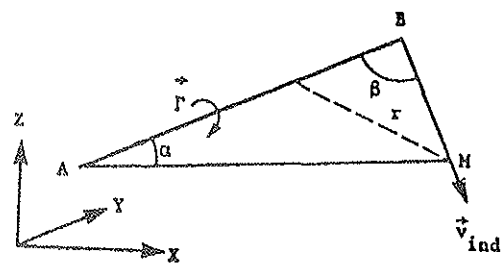


FIG.3 : Induced velocity from a line vortex

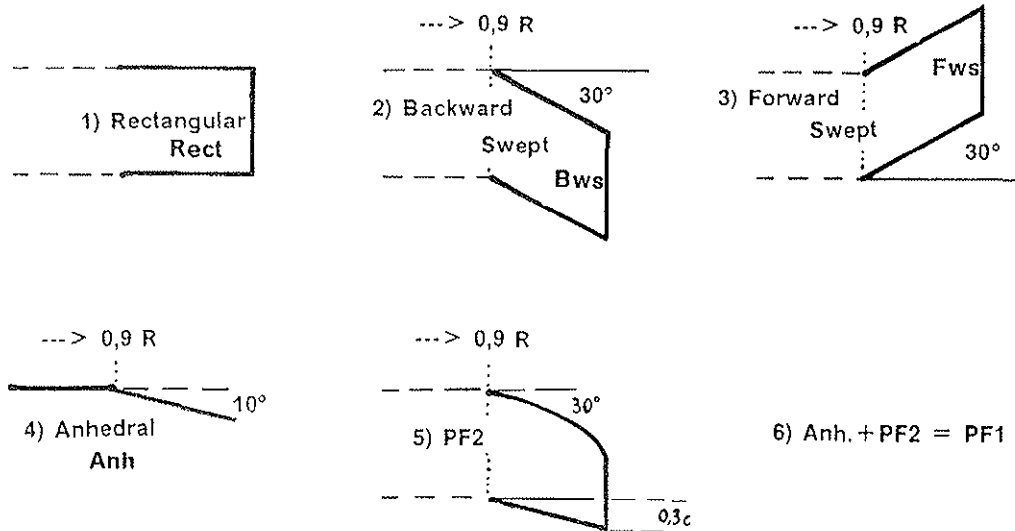


FIG.4 : Sketch of the 6 used Blade tips

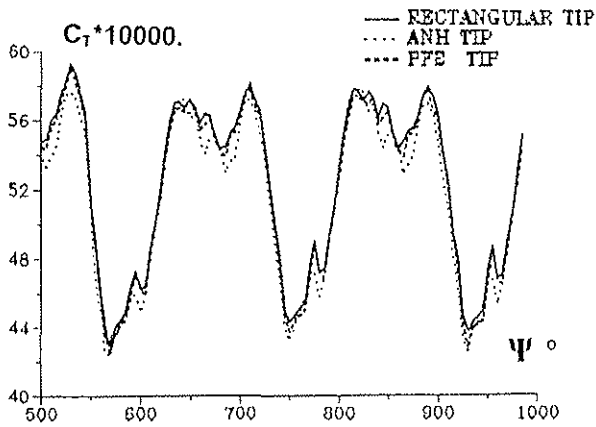


FIG.5 : Evolution of the thrust coefficient (cyclic pitch: $1^\circ 97,1^\circ$)

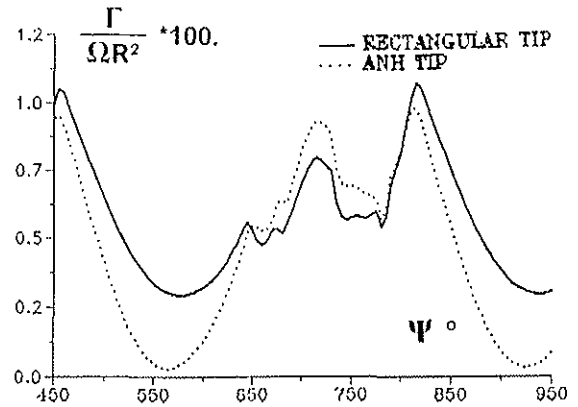


FIG.6 : Evolution of the circulation of the tip vortex

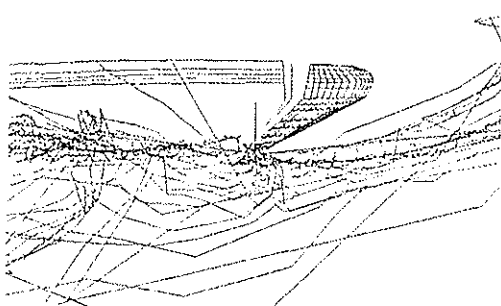


FIG.7 : Tip Vortex position for $\Psi = 775^\circ$ (PF2 tip)

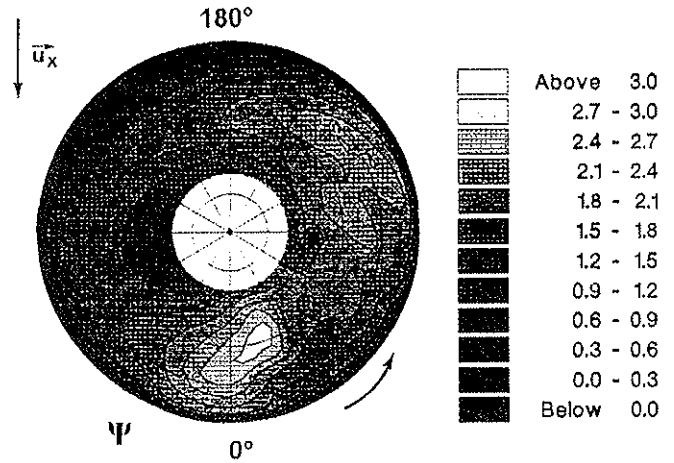


FIG.8 : Distribution of the circulation on the rotor disk (Rect tip)

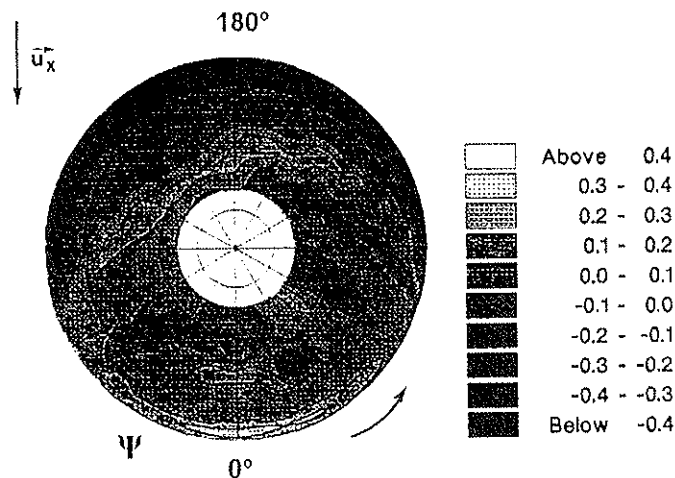


FIG.9 : Distribution of the circulation on the rotor disk : Difference between the Anhedral tip and the rectangular tip

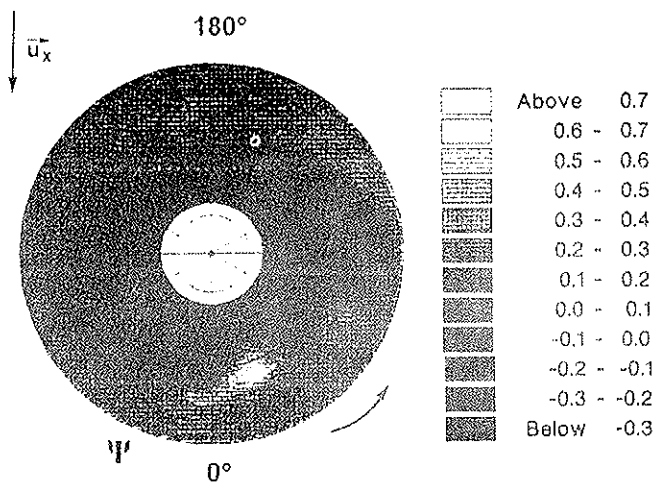


FIG.10 : Distribution of the circulation shedded in the wake during one rotor revolution (Rect tip)

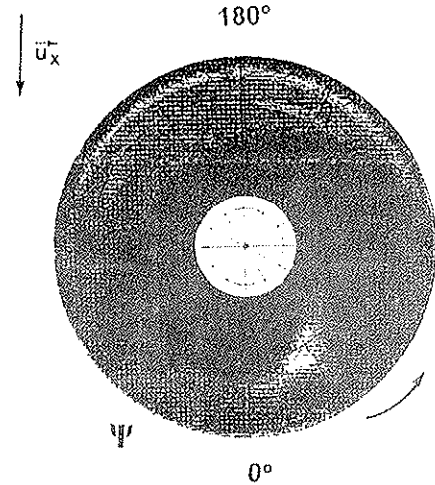


FIG.11 : PF1 tip (see FIG.10)

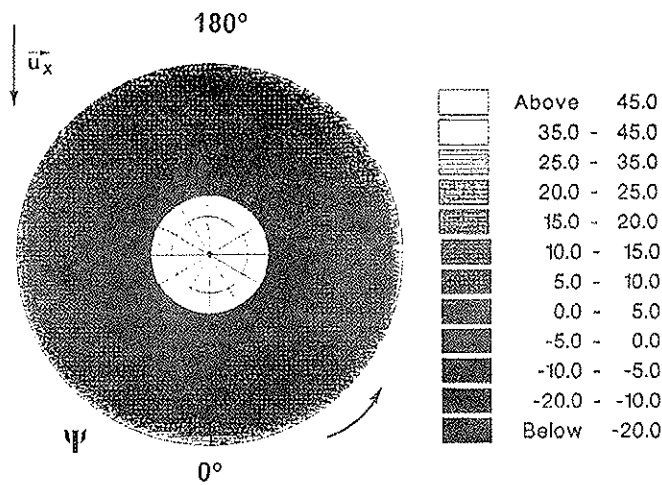


FIG.12 : Gradient of the circulation shedded in the wake (Rect tip)

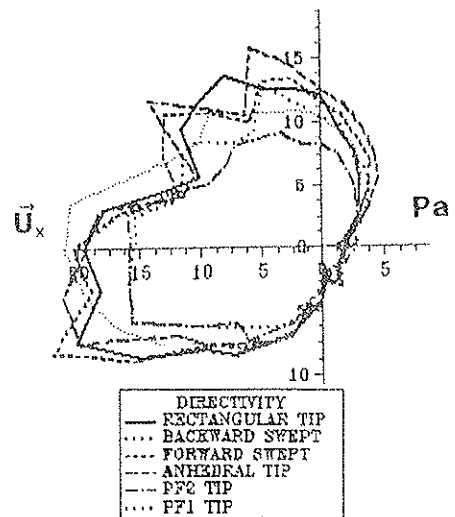


FIG.13 : Horizontal directivities of the Loading Noise for $\Phi = 0^\circ$

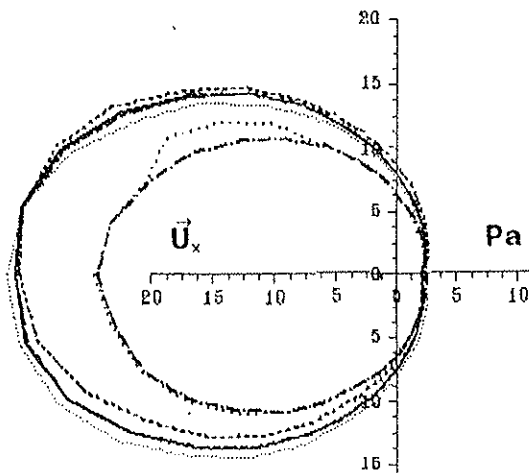


FIG.14 : Horizontal directivities of the Thickness Noise for $\Phi = 0^\circ$

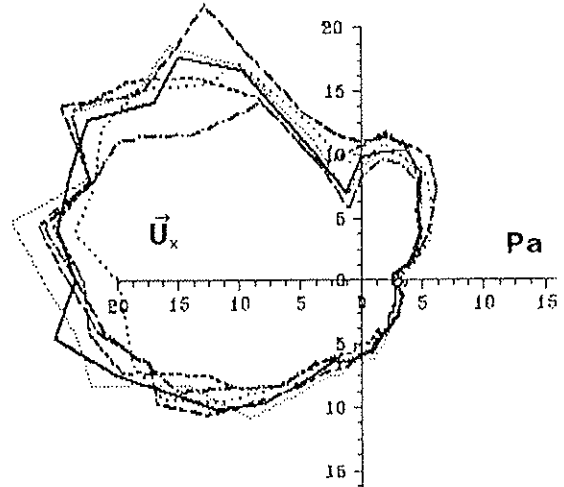


FIG.15 : Horizontal directivities of the Total Noise for $\Phi = 0^\circ$

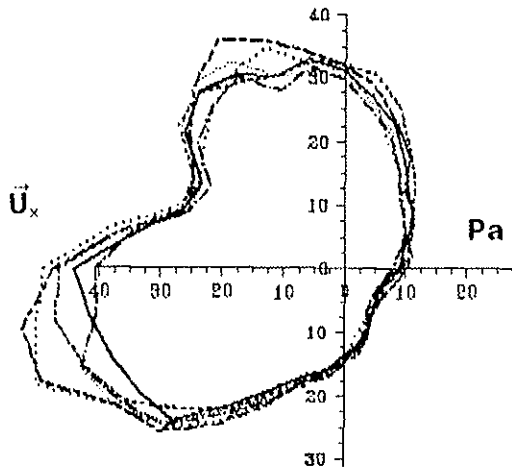


FIG.16 : Horizontal directivities of the Total Noise for $\Phi = -30^\circ$

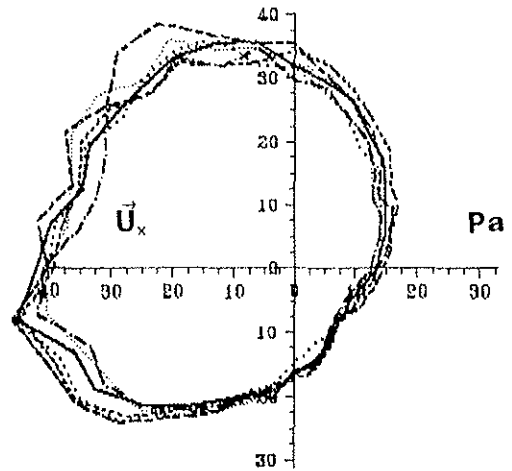


FIG.17 : Horizontal directivities of the Total Noise for $\Phi = -45^\circ$

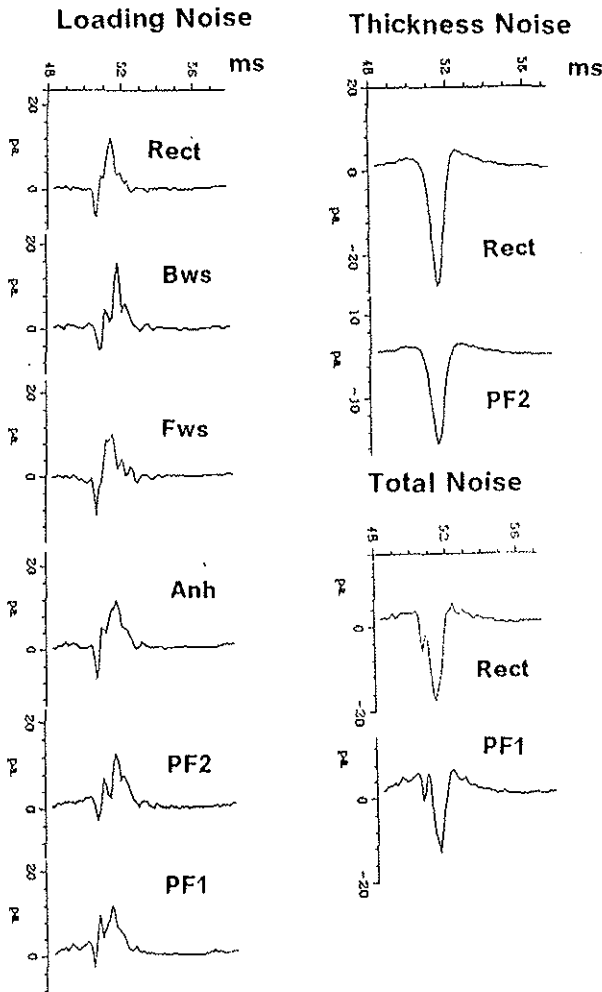


FIG.18 : Noise signatures for $\Theta = 0^\circ$ and $\Phi = 0^\circ$

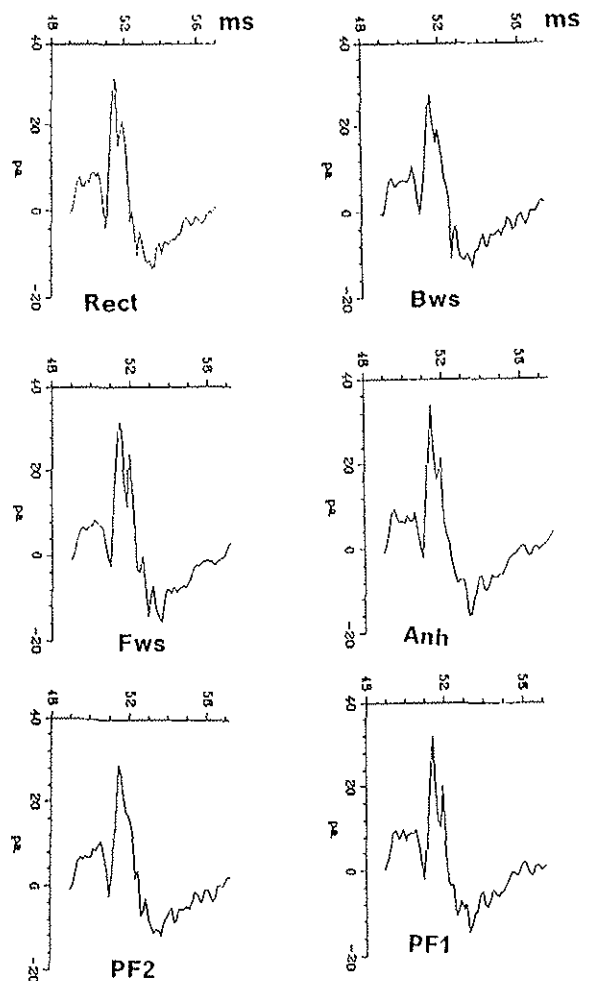


FIG.19 : Noise signatures for $\Theta = 0^\circ$ and $\Phi = -30^\circ$

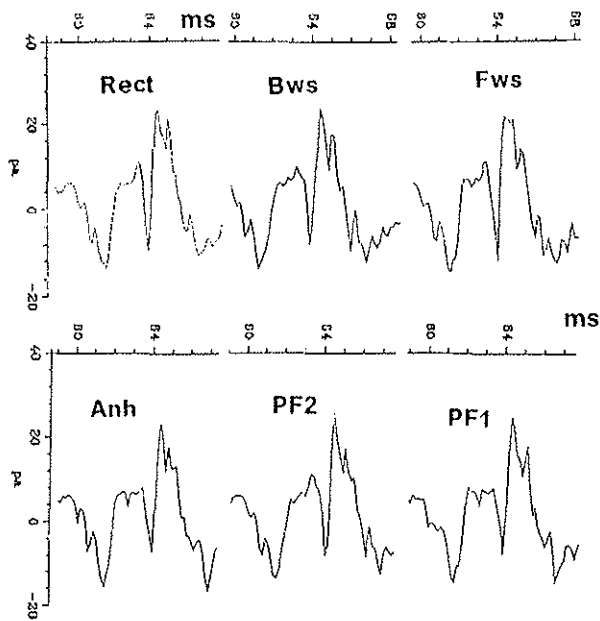


FIG.20 : Noise signatures for $\Theta = 0^\circ$ and $\Phi = -45^\circ$

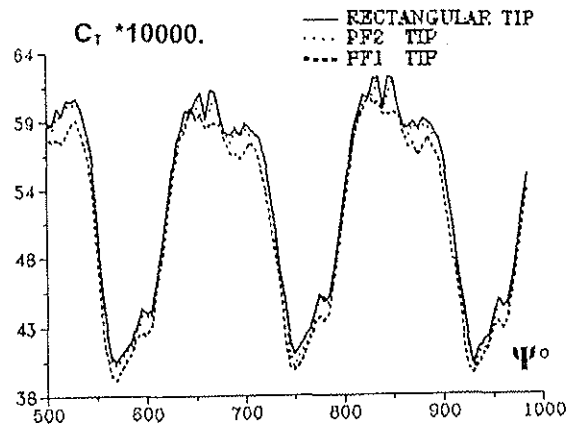


FIG.21 : Evolution of the thrust coefficient (cyclic pitch: $1^\circ, 1^\circ 97$)

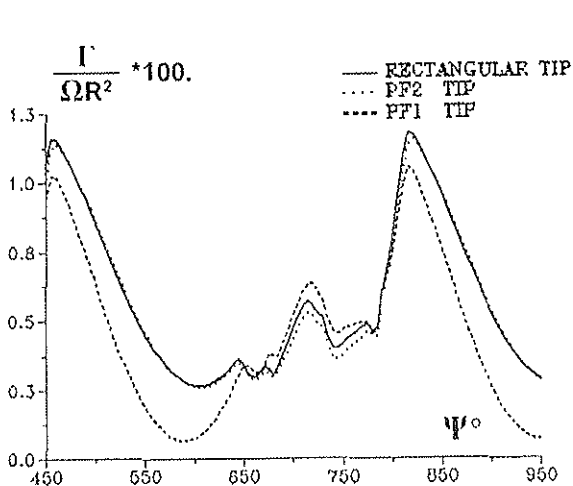


FIG.22 : Evolution of the circulation of the tip vortex

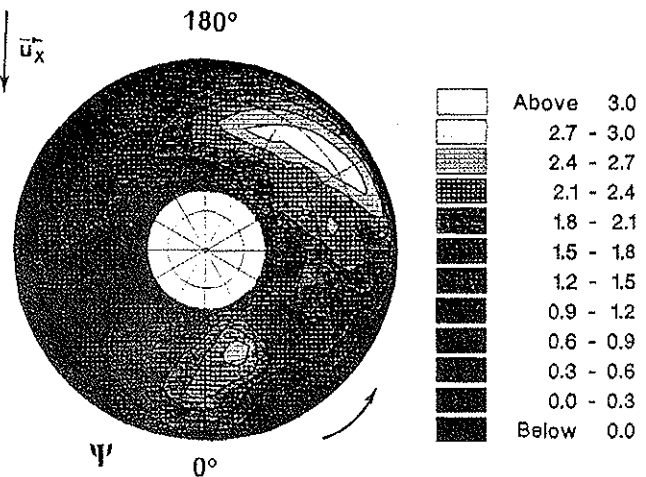


FIG.23 : Distribution of the circulation on the rotor disk (Rect tip)

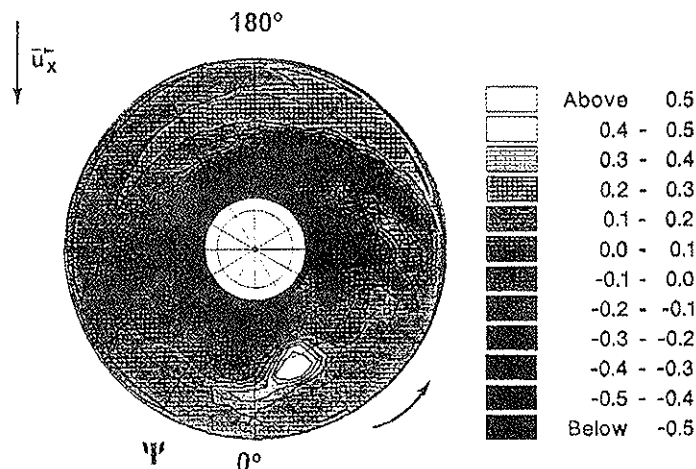


FIG.24 : Distribution of the circulation shed in the wake during one rotor revolution (Rect tip)

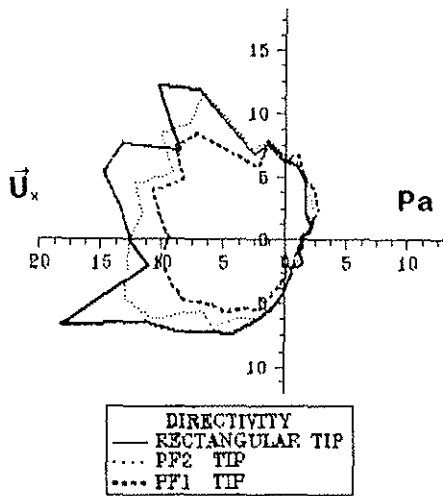


FIG.25 : Horizontal directivities of the Loading Noise for $\phi = 0^\circ$

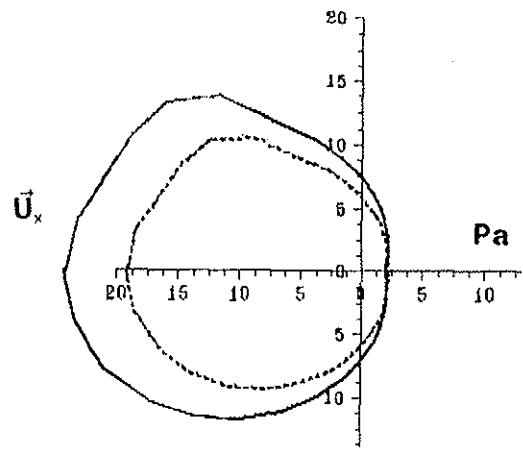


FIG.26 : Horizontal directivities of the Thickness Noise for $\phi = 0^\circ$

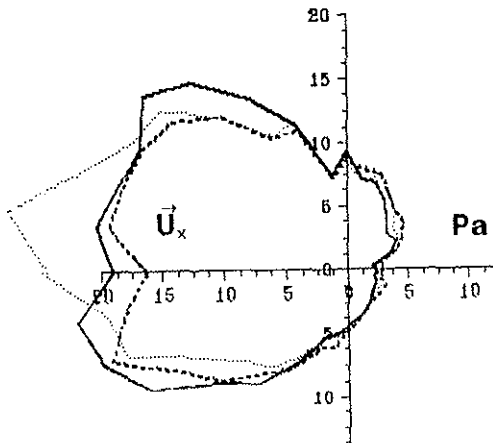


FIG.27 : Horizontal directivities of the Total Noise for $\phi = 0^\circ$

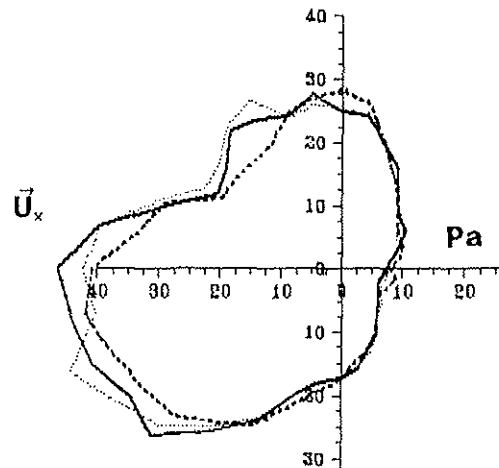


FIG.28 : Horizontal directivities of the Total Noise for $\phi = -30^\circ$

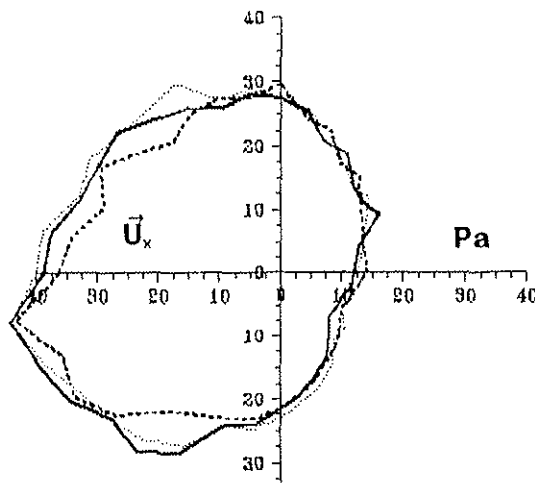


FIG.29 : Horizontal directivities of the Total Noise for $\phi = -45^\circ$

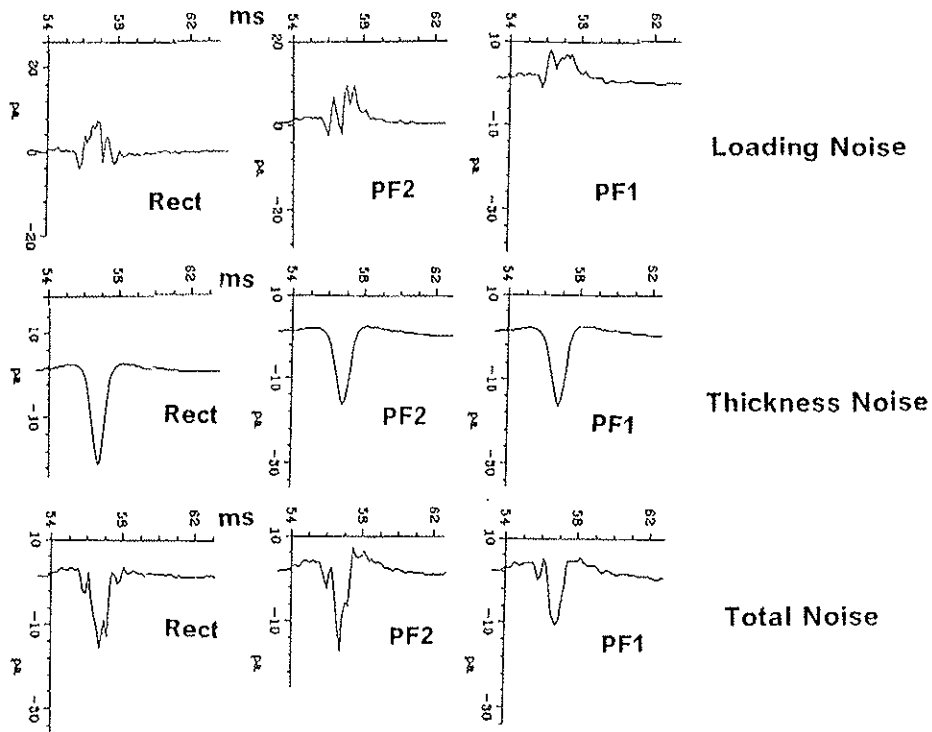


FIG.30 : Noise signatures for $\Theta = 0^\circ$ and $\Phi = 0^\circ$

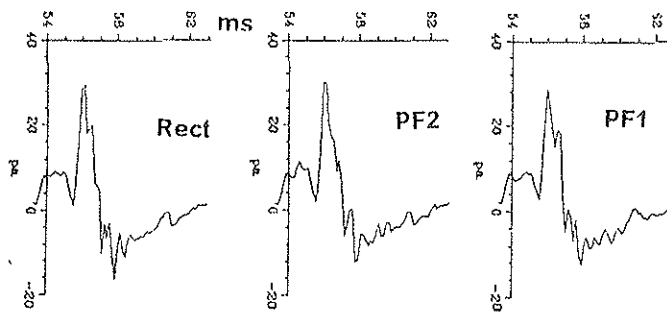


FIG.31 : Noise signatures for $\Theta = 0^\circ$ and $\Phi = -30^\circ$

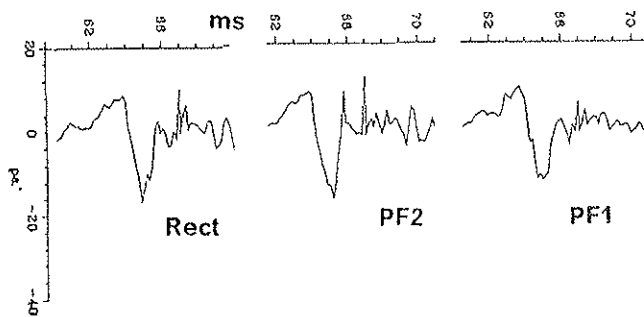


FIG.32 : Noise signatures for $\Theta = 0^\circ$ and $\Phi = -45^\circ$